

A Complete Two-Loop, Five-Gluon Helicity Amplitude in Yang-Mills Theory

Simon Badger,^a Gustav Mogull,^a Alexander Ochirov,^a Donal O'Connell^{a,b}

^a*Higgs Centre for Theoretical Physics, School of Physics and Astronomy,
The University of Edinburgh, Edinburgh EH9 3JZ, Scotland, UK*

^b*Kavli Institute for Theoretical Physics,
University of California, Santa Barbara, CA 93106-4030, USA*

E-mail: sbadger@staffmail.ed.ac.uk, g.mogull@ed.ac.uk,
alexander.ochirov@ed.ac.uk, donal@staffmail.ed.ac.uk

ABSTRACT: We compute the integrand of the full-colour, two-loop, five-gluon scattering amplitude in pure Yang-Mills theory with all helicities positive, using generalized unitarity cuts. Tree-level BCJ relations, satisfied by amplitudes appearing in the cuts, allow us to deduce all the necessary non-planar information for the full-colour amplitude from known planar data. We present our result in terms of irreducible numerators, with colour factors derived from the multi-peripheral colour decomposition. Finally, the leading soft divergences are checked to reproduce the expected infrared behaviour.

Contents

1	Introduction	1
2	Review of irreducible numerators	3
3	Colour decomposition	5
3.1	Multi-peripheral colour decomposition	5
3.2	Five-point, two-loop amplitude	8
4	Kinematic structure	11
4.1	Non-planar from planar	11
5	The full-colour five-gluon all-plus amplitude	15
6	Checking the soft divergences	17
6.1	Evaluating the massless double box in the soft limit	18
6.2	Soft divergences of the five-point integrals	19
7	Conclusions	21

1 Introduction

Precision measurements at the Large Hadron Collider provide detailed information about the nature of the strong interaction and its role within the Standard Model. With new data already arriving from Run II, there is a growing need for higher-precision theoretical predictions for a variety of different observables. Recent years have seen considerable progress in this respect. Our ability to make predictions in perturbative QCD now covers most of the relevant $2 \rightarrow 2$ scattering processes at next-to-next-to-leading order (NNLO) precision [1–13], as well as the example of inclusive Higgs production at N³LO [14]. Despite this, processes with more than two particles in the final state remain beyond the reach of current NNLO methods.

Next-to-leading order (NLO) corrections to high multiplicity final states are by now commonplace in phenomenological studies. Such computations are possible thanks to automated techniques, which make use of integrand reduction [15], recursive techniques [16], (generalized) unitarity cuts [17–20] and the known basis of scalar integrals. Processes with up to five coloured partons [21, 22] in the final state are feasible using on-shell methods that, by only working with the physical degrees of freedom, are efficient at controlling the complexity.

Multi-loop calculations of $2 \rightarrow 2$ scattering processes [12, 23–32] have been quite successful using the more traditional approaches of Feynman diagrams and integration-by-parts identities (IBPs) [33, 34], though there are notable exceptions using unitarity cutting techniques [35–40]. The main focus for these processes has been in the evaluation of the resulting master integrals. At higher multiplicity, rapid growth in the complexity of the Feynman diagram representation motivates an alternative approach that makes use of the lessons learned during the automation of one-loop computations.

Two methods have already been explored in this direction. The first of these is maximal unitarity [41], which generalises the cutting techniques of Britto, Cachazo and Feng [19] and Forde [42] to compute the rational coefficients of the master integrals, incorporating information from IBPs. Maximal unitarity has been used to look at maximal cuts for a variety of high-multiplicity examples in four dimensions [43–50]. The second approach extends the integrand reduction program of Ossola, Papadopoulos and Pittau [15]. The initial steps in this direction [51, 52] have now developed into a deeper understanding using the language of computational algebraic geometry [53–57]. The D -dimensional extension of this method has also been understood and applied in the context of the planar two-loop, five-gluon amplitude in QCD with all helicities positive (all plus) [58].

In the context of supersymmetric theories, computational methods based on an analysis of unitarity cuts have enabled a large number of high-loop computations. Other methods have also been developed, mainly in the context of these simplified theories. For example, the colour-kinematics duality of Bern, Carrasco and Johansson (BCJ) [59, 60] has been successfully exploited to find the complete colour-dressed four-loop, four-gluon amplitude in $\mathcal{N} = 4$ supersymmetric-Yang-Mills (sYM) [61]. The two-loop, five-gluon amplitude, computed in $\mathcal{N} = 4$ sYM in ref. [62], has since been extended to the non-planar sector and cast into a complete set of numerators satisfying colour-kinematics duality [63]. The integrands in planar $\mathcal{N} = 4$ sYM are known to all loop orders [64, 65], and recent studies indicate that this simplicity may extend to the non-planar sector [66, 67].

The observation that $\mathcal{N} = 4$ sYM theory and the all-plus sector of QCD¹ are related by a dimension-shifting relation [68] suggests that the all-plus amplitude at two loops could be a useful testing ground for new techniques. Indeed, at two loops the planar sector of the all-plus amplitude was observed to be related to the $\mathcal{N} = 4$ amplitude at the integrand level in a similar pattern to the one-loop story, although additional corrections to the $\mathcal{N} = 4$ sector appeared in the form of one-loop squared (or butterfly) topologies [58]. This fact prompts the question as to how much the techniques applied in supersymmetric cases may help to simplify QCD applications.

In this article, we complete the computation of the two-loop, five-gluon, all-

¹The all-plus sector is equivalent to self-dual Yang-Mills at one loop.

plus helicity amplitude including the non-planar sector. In order to deal with the increase in complexity of the full colour amplitude, we introduce a method to find compact colour decompositions that make full use of the underlying Kleiss-Kuijff (KK) relations [69] in a similar way to the previous treatment at tree level and one loop by Del Duca, Dixon and Maltoni (DDM) [70, 71]. We then further exploit the on-shell construction of the irreducible numerators to show that all of the non-planar cuts can be obtained from the planar cuts. This is reminiscent of the colour-kinematics duality, and indeed we employ the BCJ relations [59] at tree level to relate planar and non-planar cuts.

Our paper is organised as follows. We first present the colour decomposition of the all-plus, two-loop amplitude, exploiting the multi-peripheral decomposition of the underlying tree-level amplitudes. In the next section we describe how the complete kinematic structure can be constructed using knowledge from the planar sector and tree-level identities. After describing a worked example, we present compact results for the full integrand. We perform checks of the universal soft behaviour of the amplitude by evaluating the leading $\mathcal{O}(\epsilon^{-2})$ poles of the integrals in the dimensional regularisation parameter ϵ . Finally, we draw some conclusions and discuss some future directions.

2 Review of irreducible numerators

We follow a multi-loop integrand reduction algorithm [51, 53, 54, 58, 72] which uses multivariate polynomial division to find an integrand representation of the two-loop amplitude. This section is intended as a brief overview of the approach; we encourage the reader to refer to the literature for more detailed information.

An integrand-reduced two-loop amplitude has the form

$$\mathcal{A}_n^{(2)}(\{a_i\}, \{p_i\}) = ig^{n+2} \int \frac{d^d \ell_1 d^d \ell_2}{(2\pi)^{2d}} \sum_{\Gamma} \frac{\tilde{\Delta}_{\Gamma}(\{a_i\}, \{p_i\}, \ell_1, \ell_2)}{\prod_{\alpha \in \Gamma} D_{\alpha}(\{p_i\}, \ell_1, \ell_2)}, \quad (2.1)$$

where the sum over runs over graphs Γ , which are defined by a specific set of denominators D_{α} (the set $\{\alpha\}$ labels the propagators in the graph Γ .) Associated with each graph in the sum is a colour-dressed irreducible numerator $\tilde{\Delta}_{\Gamma}$; these are functions of the external momenta p_i , the loop momenta ℓ_1 and ℓ_2 , and also of the external colour indices a_i . Each of these numerators has a colour decomposition

$$\tilde{\Delta}_{\Gamma}(\{a_i\}, \{p_i\}, \ell_1, \ell_2) = \sum_{\sigma} \sigma \circ \left[C_{\Gamma}(\{a_i\}) \Delta_{\Gamma}(\{p_i\}, \ell_1, \ell_2) \right], \quad (2.2)$$

where we must explicitly determine the permutation sum σ and the associated colour factors C_{Γ} . We will present an algorithm to find a simple colour decomposition for our Yang-Mills amplitudes in the next section.

An irreducible numerator $\Delta_\Gamma(\{p_i\}, \ell_1, \ell_2)$ can be written in terms of monomials of irreducible scalar products (ISPs). To determine a set of ISPs, we first choose a spanning set of momenta to expand the scalar products along the lines of the van Neerven-Vermaseren basis [73]. By re-expressing the propagators in terms of this spanning set of scalar products, we can see that many can be written as linear combinations of propagators and can therefore be removed and pushed down into simpler topologies. These scalar products are known as reducible scalar products (RSPs.) The remaining scalar products are the ISPs; in general the propagators will be quadratic functions of them. To find a basis set of ISP monomials, these additional quadratic relations are removed using polynomial division with respect to a Gröbner basis of the relations. This technique has been developed in the public code BASISDET [53]. When working in $d = 4 - 2\epsilon$ dimensions we also include three extra-dimensional ISPs

$$\mu_{ij} = \ell_i^{[-2\epsilon]} \cdot \ell_j^{[-2\epsilon]}. \quad (2.3)$$

Once a basis set of ISP monomials is identified, their rational coefficients are computed from the generalized unitarity cuts of the amplitude. As we take all the propagators contained in a particular graph on shell, the cut amplitude factorises into a product of tree-level amplitudes summed over internal helicity states. Following our schematic notation we can write this as

$$\begin{aligned} \text{Cut}_\Gamma &= \left[\sum_{h_i} \prod_{\alpha \in \Gamma} A^{(0)}(\alpha, \{h_i\}) \right]_{\text{cut}(\Gamma)} \\ &= \left[\Delta_\Gamma(\{p_i\}, \ell_1, \ell_2) - \sum_{\Gamma' \supset \Gamma} \frac{\Delta_{\Gamma'}(\{p_i\}, \ell_1, \ell_2) \prod_{\alpha \in \Gamma} D_\alpha(\{p_i\}, \ell_1, \ell_2)}{\prod_{\alpha \in \Gamma'} D_\alpha(\{p_i\}, \ell_1, \ell_2)} \right]_{\text{cut}(\Gamma)}, \end{aligned} \quad (2.4)$$

where the trees $A^{(0)}$ are those associated with each vertex in the graph Γ . Making the distinction between the cut associated with a graph Γ and the irreducible numerator associated with the same graph is crucial for understanding this construction. The irreducible numerator contains only that information which is required on the cut associated with Γ , and which is not captured by irreducible numerators of graphs Γ' that are “larger” than Γ , in the sense that the propagators contained in Γ' are a proper superset of the propagators contained in Γ . In other words, by applying the cuts in a top-down approach we can isolate each topology systematically subtracting the higher-point singularities.

We will frequently specify the irreducible numerator associated with a graph Γ as $\Delta(\Gamma)$ for clarity; one should remember that the function $\Delta(\Gamma)$ depends on loop and external momenta. Furthermore, throughout this paper we will adopt an index notation for the graph labels which lists the number of propagators in each of the three two-loop branches ℓ_1 , ℓ_2 and $\ell_1 + \ell_2$. In addition, we add extra labels to distinguish between topologies of this type. We follow the convention that the right branch is first index, the left branch the second and finally the central branch in

the last entry. For example, the planar pentagon-box reads $\Delta_{431} = \Delta(\text{pentagon-box})$, while double box with five legs in a non-planar ordering is written $\Delta_{331;5L_2} = \Delta(\text{double box})$. A complete dictionary between this nomenclature and the graphs relevant for our two-loop, five-point calculation is given in Table 1.

As shown in ref. [58], there is only ever a single branch to the set of solutions to the on-shell equation in d dimensions, which simplifies the inversion of the system in eq. (2.4) to find the coefficients of the ISP monomials in Δ_Γ , though at the cost of an increased number of monomials with respect to the four-dimensional case.

There are two important remarks about this construction. The integrand representation of eq. (2.1) is not unique, and there are different choices for both the set of ISPs and the set of monomials. Different sets of spanning vectors will result in different ISPs and the polynomial division requires a choice of monomial ordering.

In the following sections we will exploit two important consequences of this approach. Firstly, we will restrict the form of our irreducible numerators to ensure that the choice of ISPs and monomials satisfy the basic symmetries required by our colour decompositions. Secondly, we will make use of the factorisation of irreducible numerators into ordered tree-level amplitudes. These tree amplitudes satisfy a number of relationships among different orderings. This fact will allow us to determine all non-planar cuts of the two-loop all-plus amplitude from the planar irreducible numerators computed in ref. [58].

3 Colour decomposition

The main result of this work is the construction of the complete five-point, two-loop, all-plus amplitude in Yang-Mills theory. As we mentioned in Section 2, it is necessary to choose a particular colour decomposition. This decomposition picks a set of colour tensors describing the colour structure of the amplitude. At the same time, it specifies an associated set of cut diagrams which must be computed. Each of these cut diagrams is, in turn, associated with a unique irreducible numerator. Thus the colour decomposition that we pick is of central importance, because it determines the set of irreducible numerators that we need to calculate.

In this section, we describe the general algorithm that we used for constructing an appropriate colour decomposition of the amplitude, before applying this algorithm to the specific case of the two-loop five-point amplitude.

3.1 Multi-peripheral colour decomposition

Our algorithm is applicable to the general case of an L -loop Yang-Mills amplitude. Following the generalized unitarity principle, we begin by writing the amplitude as a sum over all colour-dressed cuts. Diagrammatically, these cuts consist of vertices formed from colour-dressed tree amplitudes which are joined by on-shell propagators. At two loops the set of colour-dressed cuts can be classified by two basic topologies:

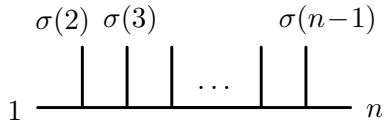


Figure 1: Multi-peripheral diagram for the colour factors in eq. (3.1).

the genuine two-loop topologies are shown in figure 2, and the one-loop squared (or butterfly) topologies in figure 3.

The central idea is to build the loop-level colour decomposition using knowledge of the underlying tree-level amplitudes. There are a variety of well-known presentations of these trees. We find it convenient to use the DDM form [70, 71] for the tree amplitudes:

$$\mathcal{A}_n^{(0)} = -ig^{n-2} \sum_{\sigma \in S_{n-2}} \tilde{f}^{a_1 a_{\sigma(2)} b_1} \tilde{f}^{b_1 a_{\sigma(3)} b_2} \dots \tilde{f}^{b_{n-4} a_{\sigma(n-2)} b_{n-3}} \tilde{f}^{b_{n-3} a_{\sigma(n-1)} a_n} \times A^{(0)}(1, \sigma(2), \dots, \sigma(n-1), n), \quad (3.1)$$

where $\tilde{f}^{abc} = i\sqrt{2}f^{abc}$ are proportional to the standard structure constants in $SU(N_c)$, the gauge group of our Yang-Mills theory. The main advantage of this form of the amplitude is that it contains $(n-2)!$ colour structures, as compared to $(n-1)!$ in the standard trace-based decomposition, for example. This fact helps to reduce the number of generated diagrams; in particular, an algorithm based directly on the trace decomposition of tree amplitudes generates a larger set of diagrams, some of which are rather obscure.

Each of the colour structures in the tree decomposition is a string of group theoretic structure constants \tilde{f}^{abc} . For an n -gluon amplitude the decomposition is constructed by fixing the position of any two gluons at either end of this string. The $(n-2)!$ permutations of the remaining gluons between the ends of the string form the set of colour factors each of which is associated with a colour-ordered tree of the same ordering. Pictorially, the colour structures look like combs, as shown in figure 1.

It is straightforward to build the loop colour structure from these DDM tree colour structures. The loop structure follows directly from the cut diagram: one simply inserts the DDM trees at the vertices; propagator lines connecting trees indicate that the ends of the DDM combs at either end of the propagator have the same colour index to be summed over. Notice, however, that we must pick two special lines in the DDM form of the tree amplitudes (corresponding to lines 1 and n in figure 1.) These lines are on opposite ends of the DDM colour strings, so one can informally think of this choice as picking two lines and “stretching” the colour ordered tree between these two ends. We make canonical choices of which legs to pick as special, depending on the number of propagators that connect to the three-point amplitude. These choices are:

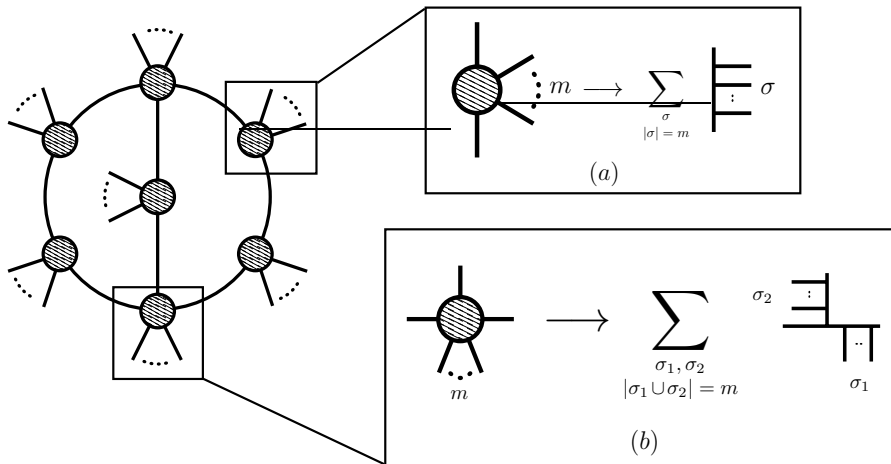


Figure 2: Inserting the DDM tree basis into the colour dressed cuts of a two-loop amplitude. The upper insert (a) shows the simple case of two loop propagators, while the lower insert (b) shows the case of three loop propagators. The sums run over the permutations of the external legs in the tree-level amplitude.

- Two propagators

In this case, it is natural to “stretch” using the two propagators as the special legs. Thus we build the colour structure by pasting a DDM multi-peripheral colour structure between the two propagators. We must sum over every ordering of the external legs. Pictorially, the operation is shown in the upper insert (a) of figure 2.

- Three propagators

In the case of three propagators, we select two out of the three propagators to be the special lines in the DDM presentation. Notice that this choice hides some of the full symmetry of the diagram. In constructing the DDM tree, the propagators we have selected must be at the end of the multi-peripheral structure; we must sum over the positions of the other legs. The result is a sum of diagrams, as shown in the lower insert (b) of figure 2.

- Four propagators

We again choose two propagators to “stretch” the cut amplitude into a DDM tree. At two loops, we only encounter this case in the butterfly topologies. We choose upper and lower propagators on the right side of the diagram as special; by symmetry, the result is the same as if we chose upper and lower propagators on the left of the diagram. The insert of figure 3 sketches out the procedure.

In this way, we build a set of colour structures. The kinematic structure associated with each colour structure is easily understood. Each time we insert a particular

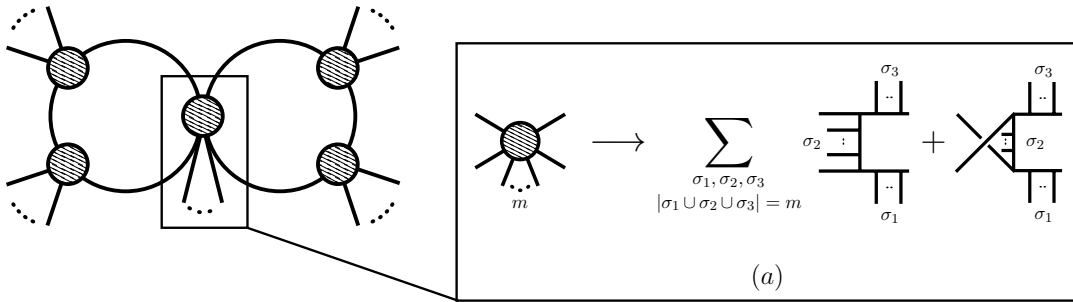


Figure 3: Inserting the DDM tree basis into a colour dressed cut of a butterfly topology at two-loops. There are four loop propagators in this case, and the insert (a) shows the result of inserting the DDM tree decomposition fixing the two right legs. The sums run over the permutations of the external legs in the tree-level amplitude.

DDM colour trace, we also pick up a factor of the associated colour-ordered tree amplitude. Thus, the orientation of the legs in the kinematic diagram, associated to an irreducible numerator, is the same as in the colour structure; of course, the “stretching” procedure does not produce new propagators in the irreducible numerator.

One advantage of using the DDM presentation of the amplitude at tree level is that the KK relations are automatically satisfied. Our procedure recycles this property to loop level: we automatically generate a set of colour diagrams that is KK-independent. Along the way, we generate ordered diagrams for the kinematics. The same procedure works at L loops; the amplitude is expressed as

$$\mathcal{A}_n^{(L)} = i^{L-1} g^{n+2L-2} \sum_{\substack{\text{KK-independent} \\ \text{1PI graphs } \Gamma_i}} \int \prod_{j=1}^L \frac{d^d \ell_j}{(2\pi)^d} \frac{1}{S_i} \frac{C_i \Delta_i(\ell)}{D_i(\ell)}, \quad (3.2)$$

where S_i are the symmetry factors of the graphs, D_i denote the products of the (inverse scalar) propagators, and the Δ_i are irreducible numerators for appropriate colour factors C_i generated through our algorithm. Now let us see this procedure at work in the context of the five-point, two-loop amplitude, which is our main focus.

3.2 Five-point, two-loop amplitude

Now we describe the colour structure of the five-point, two-loop amplitude. We concentrate on the diagrams that do not vanish in the all-plus case according to ref. [58] and our calculations in section 4. A generic five-point two-loop amplitude can be constructed by a straightforward extension of the present discussion.

Let us first write the amplitude and then explain its content in more detail. We

label Δ_i and their colour factors by their diagrams directly in the formula:

$$\begin{aligned}
\mathcal{A}^{(2)}(1, 2, 3, 4, 5) = & \\
ig^7 \sum_{\sigma \in S_5} \sigma \circ I \left[& C \left(\begin{array}{c} (5) \\ \diagup \quad \diagdown \\ (4) \quad (3) \end{array} \begin{array}{c} (1) \\ \diagdown \quad \diagup \\ (2) \end{array} \right) \left(\frac{1}{2} \Delta \left(\begin{array}{c} (5) \\ \diagup \quad \diagdown \\ (4) \quad (3) \end{array} \begin{array}{c} (1) \\ \diagdown \quad \diagup \\ (2) \end{array} \right) + \Delta \left(\begin{array}{c} (5) \\ \diagup \quad \diagdown \\ (4) \quad (3) \end{array} \begin{array}{c} (1) \\ \diagdown \quad \diagup \\ (2) \end{array} \right) + \frac{1}{2} \Delta \left(\begin{array}{c} (5) \\ \diagup \quad \diagdown \\ (4) \quad (3) \end{array} \begin{array}{c} (1) \\ \diagdown \quad \diagup \\ (2) \end{array} \right) \right. \\
& + \frac{1}{2} \Delta \left(\begin{array}{c} (5) \\ \diagup \quad \diagdown \\ (4) \quad (3) \end{array} \begin{array}{c} (1) \\ \diagdown \quad \diagup \\ (2) \end{array} \right) + \Delta \left(\begin{array}{c} (5) \\ \diagup \quad \diagdown \\ (4) \quad (3) \end{array} \begin{array}{c} (1) \\ \diagdown \quad \diagup \\ (2) \end{array} \right) + \frac{1}{2} \Delta \left(\begin{array}{c} (5) \\ \diagup \quad \diagdown \\ (4) \quad (3) \end{array} \begin{array}{c} (1) \\ \diagdown \quad \diagup \\ (2) \end{array} \right) \left. \right) \\
& + C \left(\begin{array}{c} (5) \\ \diagup \quad \diagdown \\ (4) \quad (3) \end{array} \begin{array}{c} (1) \\ \diagdown \quad \diagup \\ (2) \end{array} \right) \left(\frac{1}{4} \Delta \left(\begin{array}{c} (5) \\ \diagup \quad \diagdown \\ (4) \quad (3) \end{array} \begin{array}{c} (1) \\ \diagdown \quad \diagup \\ (2) \end{array} \right) + \frac{1}{2} \Delta \left(\begin{array}{c} (5) \\ \diagup \quad \diagdown \\ (4) \quad (3) \end{array} \begin{array}{c} (1) \\ \diagdown \quad \diagup \\ (2) \end{array} \right) + \frac{1}{2} \Delta \left(\begin{array}{c} (5) \\ \diagup \quad \diagdown \\ (4) \quad (3) \end{array} \begin{array}{c} (1) \\ \diagdown \quad \diagup \\ (2) \end{array} \right) \right. \\
& \left. - \Delta \left(\begin{array}{c} (5) \\ \diagup \quad \diagdown \\ (4) \quad (3) \end{array} \begin{array}{c} (1) \\ \diagdown \quad \diagup \\ (2) \end{array} \right) + \frac{1}{4} \Delta \left(\begin{array}{c} (5) \\ \diagup \quad \diagdown \\ (4) \quad (3) \end{array} \begin{array}{c} (1) \\ \diagdown \quad \diagup \\ (2) \end{array} \right) \right) \\
& + C \left(\begin{array}{c} (5) \\ \diagup \quad \diagdown \\ (4) \quad (3) \end{array} \begin{array}{c} (1) \\ \diagdown \quad \diagup \\ (2) \end{array} \right) \left(\frac{1}{4} \Delta \left(\begin{array}{c} (5) \\ \diagup \quad \diagdown \\ (4) \quad (3) \end{array} \begin{array}{c} (1) \\ \diagdown \quad \diagup \\ (2) \end{array} \right) + \frac{1}{2} \Delta \left(\begin{array}{c} (5) \\ \diagup \quad \diagdown \\ (4) \quad (3) \end{array} \begin{array}{c} (1) \\ \diagdown \quad \diagup \\ (2) \end{array} \right) \right) + \dots \left. \right], \tag{3.3}
\end{aligned}$$

where the integration operator I acts on every Δ_i as

$$I[\Delta_i] \equiv \int \frac{d^d \ell_1 d^d \ell_2}{(2\pi)^{2d}} \frac{\Delta_i}{D_i}. \tag{3.4}$$

The explicit symmetry factors compensate for the over-counts introduced by the overall sum over permutations of external legs. For convenience, we recapitulate all these Δ_i in table 1, where for each irreducible numerator Δ_i we also show its diagram, that of its colour factor, as well as the set of its non-equivalent permutations.

The first three graphs in table 1, Δ_{431} , Δ_{332} and Δ_{422} , are the master diagrams corresponding to the maximal cuts. They are purely trivalent, thus their colour factors are unambiguously defined by their proper graphs.

The next three graphs, $\Delta_{331;M_1}$, $\Delta_{232;M_1}$ and $\Delta_{322;M_1}$, have a four-point vertex with two external and two internal edges. The two external legs automatically enter in the permutation sum with two possible orderings, hence multi-peripheral subgraphs are naturally obtained by fixing the internal lines, as in the insert (a) of figure 2. ‘‘Stretching’’ the four-point vertex by these lines gives a master graph for each colour factor.

The following two diagrams, $\Delta_{331;5L_1}$ and $\Delta_{331;5L_2}$, share the same graph structure, up to the ordering of the four-point vertex. The apparent asymmetry introduced by our selecting these two diagrams, and omitting the graph with the external leg in the right loop, is an artefact of our colour decomposition. One could make other choices; the KK relations satisfied by the trees and their symmetries ensure that any choice is valid.

To expand the four-point vertex in the ninth graph, $\Delta_{322;5L_1}$, we fixed the internal lines of the ‘‘diamond’’ subdiagram, hence its colour factor is C_{332} , but with a minus

Numerators	Graphs	Colour factors	Permutation sum
Δ_{431}			S_5 /Vertical flip
Δ_{332}			S_5 /Vertical & horizontal flip
Δ_{422}			S_5 /Vertical & diamond flip
$\Delta_{331;M_1}$			S_5
$\Delta_{232;M_1}$			S_5 /Vertical flip
$\Delta_{322;M_1}$			S_5 /Diamond flip
$\Delta_{331;5L_1}$			S_5 /Horizontal flip
$\Delta_{331;5L_2}$			S_5 /Horizontal flip
$\Delta_{322;5L_1}$			S_5
Δ_{430}			S_5 /Vertical flip
$\Delta_{330;M_1}$			S_5
$\Delta_{330;5L_1}$			S_5 /Horizontal flip
$\Delta_{330;5L_2}$			S_5 /Horizontal & vertical flip

Table 1: The irreducible numerators that are nonzero for the all-plus five-point two-loop amplitude, along with their colour factors and reduced permutation sums.

sign due to one flipped vertex. The other permutation of the four-point vertex corresponds to the same topology and is present in the overall permutation sum with the right permuted colour diagram.

The colour factor of the planar graph Δ_{430} follows in a straightforward manner from our algorithm (see figure 3), yielding C_{431} as its colour factor. Its descendant $\Delta_{330;M_1}$ is more interesting, since it is the only graph in the all-plus case with two four-point vertices. They can be treated independently by linearity of colour decom-

position. The external one is thus expanded in the same way as in $\Delta_{331;M_1}$, producing C_{430} as an intermediate step. Expanding the internal four-point vertex gives C_{431} again.

The last two graphs, $\Delta_{330;5L_1}$ and $\Delta_{330;5L_2}$, share a five-point vertex. To explain their colour factors, let us consider the corresponding colour-dressed cut:

$$\begin{aligned}
\text{Cut}_{330;5L} = & C \left(\text{Diagram 1} \right) \text{Cut} \left(\text{Diagram 2} \right) + C \left(\text{Diagram 3} \right) \text{Cut} \left(\text{Diagram 4} \right) \\
& + C \left(\text{Diagram 5} \right) \text{Cut} \left(\text{Diagram 6} \right) + C \left(\text{Diagram 7} \right) \text{Cut} \left(\text{Diagram 8} \right) \\
& + C \left(\text{Diagram 9} \right) \text{Cut} \left(\text{Diagram 10} \right) + C \left(\text{Diagram 11} \right) \text{Cut} \left(\text{Diagram 12} \right).
\end{aligned} \tag{3.5}$$

We obtain the multi-peripheral decomposition of the five-point vertex by fixing the two right-hand loop edges and permuting the other three edges. The graphs in the second line can be vertically flipped to put leg 3 downstairs to match the presentation in table 1. Obviously, an equivalent decomposition could be achieved by fixing the loop edges on the left, which would change the orientation of leg 3 in the superficially non-planar graphs $\Delta_{330;5L_2}$. The S_5 -summation in eq. (3.3) effectively symmetrises the colour structure over the two choices of multi-peripheral decompositions.

In the present paper we can avoid lower levels of the graph hierarchy thanks to the simplicity of the fully symmetric helicity configuration, but it already incorporates all the key elements of the general colour structure.

4 Kinematic structure

With our colour decomposition at hand, we turn our attention to the kinematic structure of the amplitude. We need to compute an irreducible numerator associated to each diagram in eq. (3.3); as Frellesvig, Zhang and one of the current authors have already computed all the planar irreducible numerators [58], our task is to determine the remaining non-planar numerators. Of course, these numerators can be computed directly from their cuts. However, as we will see, it is easy to determine the complete set of non-planar irreducible numerators for this amplitude from its planar numerators and the knowledge of tree-level amplitude relations.

4.1 Non-planar from planar

The non-planar numerator $\Delta_{332} = \Delta(\boxminus)$ can, of course, be obtained directly from its cut. However, we can avoid calculating this non-planar cut explicitly by relating it to a planar cut. We do so in two steps: first, we coalesce two (ordered) three-point trees into a limit of an ordered four-point tree; then we use the BCJ relations [59] satisfied by the ordered four-point tree to reorder the legs until the complete diagram becomes planar.

In more detail, we use the following well-known relation, which is satisfied by on-shell amplitudes in the cuts:

$$A^{(0)}(1, 2, -(1+2)) A^{(0)}(1+2, 3, 4) = \left\{ s_{13} A^{(0)}(1, 3, 2, 4) \right\} \Big|_{s_{12}=0},$$

$$\begin{array}{c} 4 \quad 1 \\ \diagdown \quad / \\ \bullet \text{---} \text{---} \bullet \\ / \quad \diagdown \\ 3 \quad 2 \end{array} = \left\{ s_{13} \begin{array}{c} 4 \quad 1 \\ \diagdown \quad / \\ \bullet \\ / \quad \diagdown \\ 2 \quad 3 \end{array} \right\} \Big|_{s_{12}=0}, \quad (4.1)$$

where $s_{ij} = (p_i + p_j)^2$ are the standard Mandelstam invariants. Since this identity is of central importance for us, we present a short proof. A four-point tree amplitude can be constructed from two three-point amplitudes using the BCFW recursion relation [74, 75]:

$$A^{(0)}(1, 2, 3, 4) = \frac{1}{s_{12}} \hat{A}^{(0)}(1, 2, -(1+2)) \hat{A}^{(0)}(1+2, 3, 4), \quad (4.2)$$

where hat signs on the right-hand side indicate that the amplitudes are evaluated on complex kinematics for some BCFW shift of external legs. The exact complex value of the shifted internal momentum $\widehat{(1+2)}$ is defined by the on-shell condition

$$\hat{s}_{12} = s_{12} + \alpha z = 0, \quad (4.3)$$

where the precise expression for α depends on the particular BCFW shift. The key point is that \hat{s}_{12} is a linear function of z , with the property that in the limit $s_{12} \rightarrow 0$, $z \rightarrow 0$. In this limit eq. (4.2) becomes

$$\left\{ s_{12} A^{(0)}(1, 2, 3, 4) \right\} \Big|_{s_{12}=0} = A^{(0)}(1, 2, -(1+2)) A^{(0)}(1+2, 3, 4). \quad (4.4)$$

Notice that the left-hand side contains a nonzero contribution due to the pole in s_{12} . Now we can remove the factor of s_{12} on the left-hand side of eq. (4.4) by using the BCJ amplitude relation [59],

$$s_{12} A^{(0)}(1, 2, 3, 4) = s_{13} A^{(0)}(1, 3, 2, 4). \quad (4.5)$$

This proves the identity (4.1).

We proceed by applying our identity (4.1) to tree amplitudes inside the non-planar cut, rearranging the diagram until it becomes planar. It is simplest to begin with maximal diagrams, and then to continue to topologies with fewer propagators. We will work through the calculation of Δ_{332} , displayed in Figure 4, as an example; we computed all non-planar irreducible numerators using the same technique.

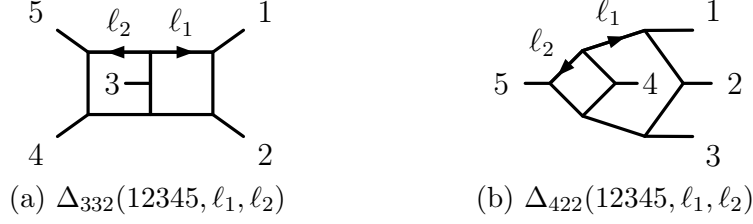


Figure 4: The two non-planar maximal topologies.

The calculation starts at the level of the cuts:

$$\begin{aligned}
\text{Cut}_{332} &= \left[\text{Diagram (a)} \right]_{(\ell_1 + \ell_2 + p_3)^2} = (\ell_1 + \ell_2 + p_3)^2 \left[\text{Diagram (a)} \right]_{(\ell_1 + \ell_2 + p_3)^2=0} \\
&= (\ell_1 - p_{123})^2 \left[\text{Diagram (b)} \right]_{(\ell_1 + \ell_2 + p_3)^2=0} = (\ell_1 - p_{123})^2 \text{Cut}_{331;5L_1} \Big|_{(\ell_1 + \ell_2 + p_3)^2=0},
\end{aligned} \tag{4.6}$$

where $p_{i\dots j} = p_i + \dots + p_j$, and we understand that all internal helicities are implicitly summed over while all exposed propagators are cut. These cuts are decomposed into irreducible numerators as

$$\text{Cut}_{332} = \Delta_{332}(12345, \ell_1, \ell_2), \tag{4.7a}$$

$$\begin{aligned}
\text{Cut}_{331;5L_1} &= \Delta_{331;5L_1}(12345, \ell_1, \ell_2) + \frac{\Delta_{431}(12345, \ell_1, \ell_2)}{(\ell_1 - p_{123})^2} \\
&\quad + \frac{\Delta_{431}(34512, p_{345} - \ell_2, p_{12} - \ell_1)}{(\ell_2 - p_{345})^2}.
\end{aligned} \tag{4.7b}$$

Using the fact that $(\ell_1 - p_{123})^2 = -(\ell_2 - p_{345})^2$ on this cut, we see that

$$\begin{aligned}
\Delta_{332}(12345, \ell_1, \ell_2) &= (\ell_1 - p_{123})^2 \Delta_{331;5L_1}(12345, \ell_1, \ell_2) + \Delta_{431}(12345, \ell_1, \ell_2) \\
&\quad - \Delta_{431}(34512, p_{345} - \ell_2, p_{12} - \ell_1).
\end{aligned} \tag{4.8}$$

A similar calculation for Δ_{422} leads to

$$\Delta_{422}(12345, \ell_1, \ell_2) = \Delta_{431}(12345, \ell_1, \ell_2). \tag{4.9}$$

So far the obtained non-planar numerators are valid only on their cuts, but they can be extended off shell. We may simply express the numerators in terms of a given set of ISPs and then define off-shell numerators unambiguously through these ISPs. The value of a given numerator depends on the choice of ISP basis off shell (in contrast to the situation on shell, of course). In this way, we determine a valid set

Graphs	ISPs	RSPs
Δ_{332}	$\ell_1 \cdot (p_5 - p_4),$ $\ell_2 \cdot (p_1 - p_2),$ $(\ell_1 - \ell_2) \cdot p_3$	$\ell_1^2, (\ell_1 - p_1)^2, (\ell_1 - p_{12})^2,$ $\ell_2^2, (\ell_2 - p_5)^2, (\ell_2 - p_{45})^2,$ $(\ell_1 + \ell_2 + p_3)^2, (\ell_1 + \ell_2)^2$
Δ_{422}	$(\ell_1 + 2\ell_2) \cdot (p_1 - p_3),$ $(\ell_1 + 2\ell_2) \cdot p_2,$ $\ell_1 \cdot (p_5 - p_4)$	$\ell_1^2, (\ell_1 - p_1)^2, (\ell_1 - p_{12})^2, (\ell_1 - p_{123})^2,$ $\ell_2^2, (\ell_2 - p_5)^2,$ $(\ell_1 + \ell_2 + p_4)^2, (\ell_1 + \ell_2)^2$

Table 2: The choices of ISPs and RSPs for the two non-planar masters, where the RSPs are chosen as the propagators of the respective graphs. Additionally, the higher-dimensional ISPs μ_{ij} are shared by all topologies.

of non-planar irreducible numerators. Notice that the ISP monomial choices made in the planar sector, such as the higher powers of μ_{ij} preferred over high powers of $(\ell_i \cdot p_j)$, will then be easily translated to the non-planar numerators.

It is very useful to maintain the symmetries of the underlying graphs in this off-shell continuation. We achieve this by choosing an appropriate basis of ISPs on a graph-by-graph basis. One engineers the ISP basis such that the loop momentum-dependence of each irreducible numerator is captured by a set of ISPs, which map into one another under the graph symmetries without using any cut conditions. The symmetries of the maximal non-planar graphs, for example, are

$$\Delta_{332}(12345, \ell_1, \ell_2) = -\Delta_{332}(21354, p_{12} - \ell_1, p_{45} - \ell_2) = \Delta_{332}(54321, \ell_2, \ell_1), \quad (4.10a)$$

$$\Delta_{422}(12345, \ell_1, \ell_2) = -\Delta_{422}(32145, p_{123} - \ell_1, p_5 - \ell_2) = \Delta_{422}(12354, \ell_1, -\ell_1 - \ell_2). \quad (4.10b)$$

These symmetries motivate our choices of ISPs, given in Table 2. For instance, the second symmetry of Δ_{332} in (4.10a) leads to a map of ISPs

$$\begin{aligned} \ell_1 \cdot (p_5 - p_4) &\leftrightarrow \ell_2 \cdot (p_1 - p_2), \\ (\ell_1 - \ell_2) \cdot p_3 &\leftrightarrow -(\ell_1 - \ell_2) \cdot p_3. \end{aligned} \quad (4.11)$$

After we express loop-momentum dependence in eqs. (4.8) and (4.9) in terms of the ISPs of Table 2, using the fact that the RSPs (cut propagators) are zero on shell, we are left with appropriate off-shell irreducible numerators. These are listed in Section 5. Note that the function Δ_{422} is not the same as the function Δ_{431} despite the on-shell equation (4.9): different ISPs are chosen to make different off-shell symmetries manifest.

We obtained irreducible numerators for lower-level non-planar diagrams in the same way, using the BCJ relations on cuts and extending the results off shell. For the all-plus amplitude at hand we find that many lower-level irreducible numerators vanish. In other words, the higher-level numerators capture the unitarity cut structure of the full amplitude, which is given below.

5 The full-colour five-gluon all-plus amplitude

In this section we present a complete summary of all kinematic numerators contributing to the colour decomposition in eq. (3.3). We include both planar [58] and non-planar irreducible numerators computed using the technique described in Section 4.1. The result is presented unrenormalized including the dependence on the spin dimension D_s of the gluon, which is equal to 4 in the FDH scheme and $4 - 2\epsilon$ in CDR [37]. The dependence on the extra dimensional ISPs $\mu_{ij} = \ell_i^{[-2\epsilon]} \cdot \ell_j^{[-2\epsilon]}$ can be collected into three general functions,

$$F_1 = (D_s - 2)(\mu_{11}\mu_{22} + (\mu_{11} + \mu_{22})^2 + 2(\mu_{11} + \mu_{22})\mu_{12}) + 16(\mu_{12}^2 - \mu_{11}\mu_{22}), \quad (5.1a)$$

$$F_2 = 4(D_s - 2)(\mu_{11} + \mu_{22})\mu_{12}, \quad (5.1b)$$

$$F_3 = (D_s - 2)^2 \mu_{11}\mu_{22}. \quad (5.1c)$$

The remaining coefficients are expressed using the standard spinor-helicity formalism. In particular, we denote

$$\begin{aligned} \text{tr}_5 &= 4i\epsilon_{\mu\nu\rho\sigma} p_1^\mu p_2^\nu p_3^\rho p_4^\sigma \\ &= \text{tr}_+(1234) - \text{tr}_-(1234) \\ &= [12]\langle 23\rangle\langle 34\rangle\langle 41\rangle - \langle 12\rangle[23]\langle 34\rangle[41], \end{aligned} \quad (5.2)$$

since $\text{tr}_\pm = \text{tr}(\frac{1}{2}(1 \pm \gamma_5)1234)$. We also make use of ‘‘spurious’’ directions in order to find compact representations of the integrands,

$$\omega_{abc}^\mu = \frac{\langle bc\rangle[ca]}{s_{ab}} \frac{\langle a|\gamma^\mu|b\rangle}{2} - \frac{\langle ac\rangle[cb]}{s_{ab}} \frac{\langle b|\gamma^\mu|a\rangle}{2}. \quad (5.3)$$

The full amplitude reads

$$\begin{aligned} \mathcal{A}^{(2)}(1^+, 2^+, 3^+, 4^+, 5^+) &= \\ &ig^7 \sum_{\sigma \in S_5} \sigma \circ I \left[C \left(\begin{array}{c} \text{Diagram 1} \\ \text{Diagram 2} \end{array} \right) \left(\frac{1}{2}\Delta \left(\begin{array}{c} \text{Diagram 3} \\ \text{Diagram 4} \end{array} \right) + \Delta \left(\begin{array}{c} \text{Diagram 5} \\ \text{Diagram 6} \end{array} \right) + \frac{1}{2}\Delta \left(\begin{array}{c} \text{Diagram 7} \\ \text{Diagram 8} \end{array} \right) \right. \\ &\quad \left. + \frac{1}{2}\Delta \left(\begin{array}{c} \text{Diagram 9} \\ \text{Diagram 10} \end{array} \right) + \Delta \left(\begin{array}{c} \text{Diagram 11} \\ \text{Diagram 12} \end{array} \right) + \frac{1}{2}\Delta \left(\begin{array}{c} \text{Diagram 13} \\ \text{Diagram 14} \end{array} \right) \right) \\ &+ C \left(\begin{array}{c} \text{Diagram 15} \\ \text{Diagram 16} \end{array} \right) \left(\frac{1}{4}\Delta \left(\begin{array}{c} \text{Diagram 17} \\ \text{Diagram 18} \end{array} \right) + \frac{1}{2}\Delta \left(\begin{array}{c} \text{Diagram 19} \\ \text{Diagram 20} \end{array} \right) + \frac{1}{2}\Delta \left(\begin{array}{c} \text{Diagram 21} \\ \text{Diagram 22} \end{array} \right) \right. \\ &\quad \left. - \Delta \left(\begin{array}{c} \text{Diagram 23} \\ \text{Diagram 24} \end{array} \right) + \frac{1}{4}\Delta \left(\begin{array}{c} \text{Diagram 25} \\ \text{Diagram 26} \end{array} \right) \right) \\ &\quad \left. + C \left(\begin{array}{c} \text{Diagram 27} \\ \text{Diagram 28} \end{array} \right) \left(\frac{1}{4}\Delta \left(\begin{array}{c} \text{Diagram 29} \\ \text{Diagram 30} \end{array} \right) + \frac{1}{2}\Delta \left(\begin{array}{c} \text{Diagram 31} \\ \text{Diagram 32} \end{array} \right) \right) \right]. \end{aligned} \quad (5.4)$$

The three maximal graphs are

$$\begin{aligned}
\Delta_{431} &= \Delta \left(\begin{array}{c} \ell_1 \\ \text{Diagram 1} \\ 1 \\ 2 \\ 3 \\ 4 \\ 5 \end{array} \right) = -\frac{s_{12}s_{23}s_{45}F_1}{\langle 12 \rangle \langle 23 \rangle \langle 34 \rangle \langle 45 \rangle \langle 51 \rangle \text{tr}_5} \left(\text{tr}_+(1345)(\ell_1 + p_5)^2 + s_{15}s_{34}s_{45} \right), \\
\Delta_{332} &= \Delta \left(\begin{array}{c} \ell_2 \quad \ell_1 \\ \text{Diagram 2} \\ 1 \\ 2 \\ 3 \\ 4 \\ 5 \end{array} \right) = \frac{s_{12}s_{45}F_1}{4\langle 12 \rangle \langle 23 \rangle \langle 34 \rangle \langle 45 \rangle \langle 51 \rangle \text{tr}_5} \\
&\quad \times \left(s_{23}\text{tr}_+(1345)(2s_{12} - 4\ell_1 \cdot (p_5 - p_4) + 2(\ell_1 - \ell_2) \cdot p_3) \right. \\
&\quad \quad \left. - s_{34}\text{tr}_+(1235)(2s_{45} - 4\ell_2 \cdot (p_1 - p_2) - 2(\ell_1 - \ell_2) \cdot p_3) \right. \\
&\quad \quad \left. - 4s_{23}s_{34}s_{15}(\ell_1 - \ell_2) \cdot p_3 \right), \\
\Delta_{422} &= \Delta \left(\begin{array}{c} \ell_1 \\ \text{Diagram 3} \\ 1 \\ 2 \\ 3 \\ 4 \\ 5 \end{array} \right) = -\frac{s_{12}s_{23}s_{45}F_1}{\langle 12 \rangle \langle 23 \rangle \langle 34 \rangle \langle 45 \rangle \langle 51 \rangle \text{tr}_5} \\
&\quad \times \left(\text{tr}_+(1345) \left(\ell_1 \cdot (p_5 - p_4) - \frac{s_{45}}{2} \right) + s_{15}s_{34}s_{45} \right).
\end{aligned} \tag{5.5}$$

Meanwhile, the graphs at level 1 are

$$\begin{aligned}
\Delta_{430} &= \Delta \left(\begin{array}{c} \ell_2 \quad \ell_1 \\ \text{Diagram 4} \\ 1 \\ 2 \\ 3 \\ 4 \\ 5 \end{array} \right) = -\frac{s_{12}\text{tr}_+(1345)}{2\langle 12 \rangle \langle 23 \rangle \langle 34 \rangle \langle 45 \rangle \langle 51 \rangle s_{13}} (2(\ell_1 \cdot \omega_{123}) + s_{23}) \\
&\quad \times \left(F_2 + F_3 \frac{(\ell_1 + \ell_2)^2 + s_{45}}{s_{45}} \right), \\
\Delta_{331;5L_1} &= \Delta \left(\begin{array}{c} \text{Diagram 5} \\ 1 \\ 2 \\ 3 \\ 4 \\ 5 \end{array} \right) = \frac{s_{12}s_{23}s_{34}s_{45}s_{51}F_1}{\langle 12 \rangle \langle 23 \rangle \langle 34 \rangle \langle 45 \rangle \langle 51 \rangle \text{tr}_5}, \\
\Delta_{331;5L_2} &= \Delta \left(\begin{array}{c} \text{Diagram 6} \\ 1 \\ 2 \\ 3 \\ 4 \\ 5 \end{array} \right) = -\frac{s_{12}s_{45}F_1}{4\langle 12 \rangle \langle 23 \rangle \langle 34 \rangle \langle 45 \rangle \langle 51 \rangle \text{tr}_5} \\
&\quad \times (2s_{23}s_{34}s_{15} - s_{23}\text{tr}_+(1345) + s_{34}\text{tr}_+(1235)), \\
\Delta_{322;5L_1} &= \Delta \left(\begin{array}{c} \text{Diagram 7} \\ 1 \\ 2 \\ 3 \\ 4 \\ 5 \end{array} \right) = -\frac{s_{12}F_1}{2\langle 12 \rangle \langle 23 \rangle \langle 34 \rangle \langle 45 \rangle \langle 51 \rangle \text{tr}_5} \\
&\quad \times (s_{23}s_{45}\text{tr}_+(1435) - s_{15}s_{34}\text{tr}_+(2453)), \\
\Delta_{331;M_1} &= \Delta \left(\begin{array}{c} \text{Diagram 8} \\ 1 \\ 2 \\ 3 \\ 4 \\ 5 \end{array} \right) = \Delta_{322;M_1} = \Delta \left(\begin{array}{c} \text{Diagram 9} \\ 1 \\ 2 \\ 3 \\ 4 \\ 5 \end{array} \right) = \Delta_{232;M_1} = \Delta \left(\begin{array}{c} \text{Diagram 10} \\ 1 \\ 2 \\ 3 \\ 4 \\ 5 \end{array} \right) \\
&= -\frac{s_{34}s_{45}^2\text{tr}_+(1235)F_1}{\langle 12 \rangle \langle 23 \rangle \langle 34 \rangle \langle 45 \rangle \langle 51 \rangle \text{tr}_5},
\end{aligned} \tag{5.6}$$

Finally, the graphs at level 2 are

$$\begin{aligned}
\Delta_{330;M_1} &= \Delta \left(\text{graph} \right) = -\frac{(s_{45} - s_{12})\text{tr}_+(1345)}{2\langle 12 \rangle \langle 23 \rangle \langle 34 \rangle \langle 45 \rangle \langle 51 \rangle s_{13}} \left(F_2 + F_3 \frac{(\ell_1 + \ell_2)^2 + s_{45}}{s_{45}} \right), \\
\Delta_{330;5L_1} &= \Delta \left(\text{graph} \right) = -\frac{1}{\langle 12 \rangle \langle 23 \rangle \langle 34 \rangle \langle 45 \rangle \langle 51 \rangle} \\
&\times \left\{ \frac{1}{2} \left(\text{tr}_+(1245) - \frac{\text{tr}_+(1345)\text{tr}_+(1235)}{s_{13}s_{35}} \right) \right. \\
&\times \left(F_2 + F_3 \frac{4(\ell_1 \cdot p_3)(\ell_2 \cdot p_3) + (\ell_1 + \ell_2)^2(s_{12} + s_{45}) + s_{12}s_{45}}{s_{12}s_{45}} \right) \\
&+ F_3 \left[(\ell_1 + \ell_2)^2 s_{15} \right. \\
&+ \text{tr}_+(1235) \left(\frac{(\ell_1 + \ell_2)^2}{2s_{35}} - \frac{\ell_1 \cdot p_3}{s_{12}} \left(1 + \frac{2(\ell_2 \cdot \omega_{543})}{s_{35}} + \frac{s_{12} - s_{45}}{s_{35}s_{45}} (\ell_2 - p_5)^2 \right) \right) \\
&+ \left. \left. \text{tr}_+(1345) \left(\frac{(\ell_1 + \ell_2)^2}{2s_{13}} - \frac{\ell_2 \cdot p_3}{s_{45}} \left(1 + \frac{2(\ell_1 \cdot \omega_{123})}{s_{13}} + \frac{s_{45} - s_{12}}{s_{12}s_{13}} (\ell_1 - p_1)^2 \right) \right) \right] \right\}, \\
\Delta_{330;5L_2} &= \Delta \left(\text{graph} \right) = \frac{F_3}{2\langle 12 \rangle \langle 23 \rangle \langle 34 \rangle \langle 45 \rangle \langle 51 \rangle s_{12}} \\
&\times \left((s_{45} - s_{12})\text{tr}_+(1245) - \left(\text{tr}_+(1245) - \frac{\text{tr}_+(1345)\text{tr}_+(1235)}{s_{13}s_{35}} \right) 2(\ell_1 \cdot p_3) \right. \\
&\quad - \frac{s_{45}\text{tr}_+(1235)}{s_{35}} \left(2(\ell_2 \cdot \omega_{543}) + \frac{s_{12} - s_{45}}{s_{45}} (\ell_2 - p_5)^2 \right) \\
&\quad \left. + \frac{s_{12}\text{tr}_+(1345)}{s_{13}} \left(2(\ell_1 \cdot \omega_{123}) + \frac{s_{45} - s_{12}}{s_{12}} (\ell_1 - p_1)^2 \right) \right).
\end{aligned} \tag{5.7}$$

We have found a representation of the full amplitude with no topologies with fewer than six propagators. We note that there are nonzero cuts at the integrand level, but the resulting integrals are scaleless and hence zero in dimensional regularisation. We have checked additional cuts at levels 2 and 3 to ensure that no nonzero topologies remain. To find an integrand with this property, the ISPs $(\ell_1 \cdot \omega_{123})$ and $(\ell_2 \cdot \omega_{543})$ in the numerators $\Delta_{330;5L_2}$ and $\Delta_{330;5L_1}$ were upgraded to include terms proportional to $(\ell_1 - p_1)^2$ and $(\ell_2 - p_5)^2$.

6 Checking the soft divergences

Since the all-plus helicity configuration is zero at tree level, the universal infrared (IR) structure is the same as that of an ordinary one-loop amplitude. The poles of our two-loop amplitude should therefore be equivalent to those of the finite one-loop amplitude multiplied by the infrared pole operator including the sum over colour

correlations [76]

$$\mathcal{A}^{(2)}(1^+, 2^+, 3^+, 4^+, 5^+) = \sum_{\substack{i,j \\ j \neq i}} \frac{c_\Gamma}{\epsilon^2} \left(\frac{\mu_R^2}{-s_{ij}} \right)^\epsilon T_i \cdot T_j \circ \mathcal{A}^{(1)}(1^+, 2^+, 3^+, 4^+, 5^+) + \mathcal{O}(\epsilon^{-1}), \quad (6.1)$$

where we have used the \circ symbol to indicate that the colour matrices (in this purely gluonic case they will all be structure constants) should be inserted into the colour factors of the one-loop amplitude. The standard loop prefactor is given by ²

$$c_\Gamma = \frac{\Gamma(1+\epsilon)\Gamma^2(1-\epsilon)}{(4\pi)^{2-\epsilon}\Gamma(1-2\epsilon)}. \quad (6.2)$$

The one-loop amplitude to all orders in ϵ can be found in ref. [68].

There are a number of difficulties in checking eq. (6.1) in full since the five-point planar and non-planar integrals required are still unknown at this time. Resorting to numerical evaluation, as has been done in the planar case [58], is computationally prohibitive for two reasons. Firstly, the full colour expansion contains a large number of dimension-shifted integrals ($\sim \mathcal{O}(1000)$) – an order of magnitude more than the leading colour terms. Secondly, there is no Euclidean region for the complete amplitude, and so contour deformation must be performed for many of these integrals, making them more complicated than the planar cases. This task is probably achievable with public tools like FIESTA [77] and SECDEC [78].

There is, however, a much simpler method to check the leading soft singularities up to $\mathcal{O}(\epsilon^{-1})$, which can be done analytically. In the leading soft limit, the colour correlations drop out of eq. (6.1):

$$\mathcal{A}^{(2)}(1^+, 2^+, 3^+, 4^+, 5^+) = -\frac{5N_c c_\Gamma}{\epsilon^2} \mathcal{A}^{(1)}(1^+, 2^+, 3^+, 4^+, 5^+) + \mathcal{O}(\epsilon^{-1}). \quad (6.3)$$

Clearly this is a weaker check than the full IR poles, but it does require non-trivial properties of the non-planar sector. The butterfly (one-loop squared) topologies, are all finite and therefore not relevant for the IR properties. Scattering amplitudes in the soft or eikonal limit have many remarkable structures and universal properties. The interested reader may like to turn to ref. [79] for a recent introduction to the subject.

6.1 Evaluating the massless double box in the soft limit

The extra simplicity in our all-plus loop amplitude that sets it aside from most two-loop amplitudes is that the integrals contain at most a single soft divergence,

²The normalisation of the integrals in this section is different by a factor of $i/(4\pi)^{d/2}$ per integration with respect to the default choices in FIESTA and SECDEC.

IBP relations from FIRE5 [81].³ We have performed this task for the planar double box with an off-shell leg. Thus we arrived at the following soft limits for the integrals:

$$I^{4-2\epsilon} \left(\text{Diagram 1} \right) [F_1] = \frac{1}{(4\pi)^4} \frac{D_s - 2}{3s_{12}s_{23}\epsilon^2} + \mathcal{O}(\epsilon^{-1}), \quad (6.10a)$$

$$I^{4-2\epsilon} \left(\text{Diagram 2} \right) [F_1(\ell_1 \cdot p_5)] = \frac{1}{(4\pi)^4} \frac{(D_s - 2)(2s_{15} + s_{25})}{12s_{12}s_{23}\epsilon^2} + \mathcal{O}(\epsilon^{-1}), \quad (6.10b)$$

$$I^{4-2\epsilon} \left(\text{Diagram 3} \right) [F_1] = \mathcal{O}(\epsilon^{-1}), \quad (6.11a)$$

$$I^{4-2\epsilon} \left(\text{Diagram 4} \right) [F_1(\ell_1 \cdot (p_5 - p_4))] = \mathcal{O}(\epsilon^{-1}), \quad (6.11b)$$

$$I^{4-2\epsilon} \left(\text{Diagram 5} \right) [F_1((\ell_1 - \ell_2) \cdot p_3)] = \mathcal{O}(\epsilon^{-1}), \quad (6.11c)$$

$$I^{4-2\epsilon} \left(\text{Diagram 6} \right) [F_1] = \frac{1}{(4\pi)^4} \frac{D_s - 2}{3s_{12}s_{23}\epsilon^2} + \mathcal{O}(\epsilon^{-1}), \quad (6.12a)$$

$$I^{4-2\epsilon} \left(\text{Diagram 7} \right) [F_1(\ell_1 \cdot (p_5 - p_4))] = \frac{1}{(4\pi)^4} \frac{(D_s - 2)(s_{15} - s_{14} + s_{34} - s_{35})}{12s_{12}s_{23}\epsilon^2} + \mathcal{O}(\epsilon^{-1}), \quad (6.12b)$$

$$I^{4-2\epsilon} \left(\text{Diagram 8} \right) [F_1] = \frac{1}{(4\pi)^4} \frac{D_s - 2}{6\epsilon^2} \left(\frac{1}{s_{12}} + \frac{1}{s_{45}} \right) + \mathcal{O}(\epsilon^{-1}), \quad (6.13)$$

$$I^{4-2\epsilon} \left(\text{Diagram 9} \right) [F_1] = \frac{1}{(4\pi)^4} \frac{D_s - 2}{6s_{12}\epsilon^2} + \mathcal{O}(\epsilon^{-1}), \quad (6.14)$$

$$I^{4-2\epsilon} \left(\text{Diagram 10} \right) [F_1] = \frac{1}{(4\pi)^4} \frac{D_s - 2}{6s_{45}\epsilon^2} + \mathcal{O}(\epsilon^{-1}), \quad (6.15)$$

$$I^{4-2\epsilon} \Delta \left(\text{Diagram 11} \right) [F_1] = \frac{1}{(4\pi)^4} \frac{D_s - 2}{6s_{45}\epsilon^2} + \mathcal{O}(\epsilon^{-1}), \quad (6.16)$$

$$I^{4-2\epsilon} \left(\text{Diagram 12} \right) [F_1] = \mathcal{O}(\epsilon^{-1}). \quad (6.17)$$

Using these results, we have checked that eq. (6.3) does hold as expected for our amplitude (5.4).

³We thank Claude Duhr for providing his own computation of the integrals for $e^+e^- \rightarrow 3j$ [82, 83].

7 Conclusions

In this paper we have explored the impact of tree-level amplitude relations in multi-loop integrand computations. There were two major aspects to our work. Firstly, we exploited the Kleiss-Kuijf relations to find a compact colour decomposition for the two-loop amplitude in terms of multi-peripheral colour factors in an analogous way to the tree-level and one-loop decompositions of Del Duca, Dixon and Maltoni [70, 71].

Secondly, we applied the BCJ amplitude relations [59] to relate all non-planar generalized unitarity cuts to the previously computed planar ones. This allowed us to easily generate a compact representation the full colour two-loop, five-gluon, all-plus integrand building on previous planar work [58]. The soft infrared poles of the full amplitude were checked against the well-known universal pole structure.

We hope that the computational methods developed here will be of good use in the necessary extension to more general helicity configurations and other $2 \rightarrow 3$ scattering processes at two loops. They highlight some advantages of relating two-loop integrands to tree-level amplitudes via generalized unitarity cuts. As well as avoiding the large intermediate steps that make Feynman diagram computations at this loop order and multiplicity extremely computationally intensive, we are able to build known on-shell symmetries and relations into the amplitude by construction.

Another interesting aspect of the all-plus amplitude is the continuing connection to the previously known amplitudes in $\mathcal{N} = 4$ sYM. Though the dimension shifting relation observed at one loop no longer holds, the integrands of our full all-plus amplitude and the expressions of Carrasco and Johansson [63] are related by the same dimension shifting operator seen in the planar case. For example, we find that

$$\Delta_{xyz;T}(1^+, 2^+, 3^+, 4^+, 5^+) = \frac{F_1(\mu_{11}, \mu_{22}, \mu_{12})}{\langle 12 \rangle^4} \Delta_{xyz;T}^{[\mathcal{N}=4]}(1^-, 2^-, 3^+, 4^+, 5^+), \quad z \neq 0. \quad (7.1)$$

The one-loop squared topologies have the form

$$\Delta_{xy0;T}(1^+, 2^+, 3^+, 4^+, 5^+) = (F_1(\mu_{11}, \mu_{22}, \mu_{12}) - F_1(\mu_{11}, \mu_{22}, -\mu_{12})) A(\{p_i\}, \ell_1, \ell_2) + F_3(\mu_{11}, \mu_{22}, \mu_{12}) B(\{p_i\}, \ell_1, \ell_2), \quad (7.2)$$

where A and B are some functions of the external kinematics and loop momenta. The second term is proportional to $(D_s - 2)^2$ and is a genuine contribution in QCD not related to $\mathcal{N} = 4$. This additional numerator structure is enough to make the off-shell BCJ symmetries non-trivial to satisfy, even though the $\mathcal{N} = 4$ integrand has been cast in such a form. It is an interesting question as to whether this would be possible for the amplitudes presented here and one that we intend to explore in the future.

Acknowledgments

We would like to thank JJ Carrasco, Claude Duhr, Einar Gardi, and Henrik Johansson for useful discussions. Particular thanks go to Chris White for enlightening remarks on the soft singularities of loop integrals. SB is supported by an STFC Rutherford Fellowship ST/L004925/1. GM is supported by an STFC Studentship ST/K501980/1. AO is supported by the EU via a Marie Curie Actions grant FP7-PEOPLE-2013-CIG 631370. DOC is supported in part by the STFC consolidated grant “Particle Physics at the Higgs Centre”, by the National Science Foundation under grant NSF PHY11-25915, and by the Marie Curie FP7 grant 631370.

References

- [1] S. Catani, L. Cieri, D. de Florian, G. Ferrera, and M. Grazzini, *Diphoton production at hadron colliders: a fully-differential QCD calculation at NNLO*, *Phys. Rev. Lett.* **108** (2012) 072001, [[arXiv:1110.2375](#)].
- [2] M. Czakon, P. Fiedler, and A. Mitov, *Total Top-Quark Pair-Production Cross Section at Hadron Colliders Through $O(\frac{4}{3})$* , *Phys.Rev.Lett.* **110** (2013) 252004, [[arXiv:1303.6254](#)].
- [3] M. Czakon, P. Fiedler, and A. Mitov, *Resolving the Tevatron top quark forward-backward asymmetry puzzle*, [arXiv:1411.3007](#).
- [4] T. Gehrmann, M. Grazzini, S. Kallweit, P. Maierhofer, A. von Manteuffel, et al., *W^+W^- Production at Hadron Colliders in Next to Next to Leading Order QCD*, *Phys.Rev.Lett.* **113** (2014), no. 21 212001, [[arXiv:1408.5243](#)].
- [5] M. Grazzini, S. Kallweit, and D. Rathlev, *$W\gamma$ and $Z\gamma$ production at the LHC in NNLO QCD*, *JHEP* **07** (2015) 085, [[arXiv:1504.01330](#)].
- [6] M. Grazzini, S. Kallweit, D. Rathlev, and A. Torre, *$Z\gamma$ production at hadron colliders in NNLO QCD*, *Phys.Lett.* **B731** (2014) 204–207, [[arXiv:1309.7000](#)].
- [7] F. Cascioli, T. Gehrmann, M. Grazzini, S. Kallweit, P. Maierhofer, et al., *ZZ production at hadron colliders in NNLO QCD*, *Phys.Lett.* **B735** (2014) 311–313, [[arXiv:1405.2219](#)].
- [8] R. Boughezal, C. Focke, X. Liu, and F. Petriello, *W -boson production in association with a jet at next-to-next-to-leading order in perturbative QCD*, [arXiv:1504.02131](#).
- [9] X. Chen, T. Gehrmann, E. Glover, and M. Jaquier, *Precise QCD predictions for the production of Higgs + jet final states*, *Phys.Lett.* **B740** (2015) 147–150, [[arXiv:1408.5325](#)].
- [10] R. Boughezal, C. Focke, W. Giele, X. Liu, and F. Petriello, *Higgs boson production in association with a jet using jetiness subtraction*, *Phys.Lett.* **B748** (2015) 5–8, [[arXiv:1505.03893](#)].

- [11] R. Boughezal, F. Caola, K. Melnikov, F. Petriello, and M. Schulze, *Higgs Boson Production in Association with a Jet at Next-to-Next-to-Leading Order*, [arXiv:1504.07922](#).
- [12] E. W. N. Glover, C. Oleari, and M. E. Tejeda-Yeomans, *Two loop QCD corrections to gluon-gluon scattering*, *Nucl. Phys.* **B605** (2001) 467–485, [[hep-ph/0102201](#)].
- [13] A. G.-D. Ridder, T. Gehrmann, E. W. N. Glover, A. Huss, and T. A. Morgan, *Precise QCD predictions for the production of a Z boson in association with a hadronic jet*, [arXiv:1507.02850](#).
- [14] C. Anastasiou, C. Duhr, F. Dulat, F. Herzog, and B. Mistlberger, *Higgs Boson Gluon-Fusion Production in QCD at Three Loops*, *Phys.Rev.Lett.* **114** (2015), no. 21 212001, [[arXiv:1503.06056](#)].
- [15] G. Ossola, C. G. Papadopoulos, and R. Pittau, *Reducing full one-loop amplitudes to scalar integrals at the integrand level*, *Nucl. Phys.* **B763** (2007) 147–169, [[hep-ph/0609007](#)].
- [16] F. Cascioli, P. Maierhofer, and S. Pozzorini, *Scattering Amplitudes with Open Loops*, *Phys.Rev.Lett.* **108** (2012) 111601, [[arXiv:1111.5206](#)].
- [17] Z. Bern, L. J. Dixon, D. C. Dunbar, and D. A. Kosower, *One-Loop n-Point Gauge Theory Amplitudes, Unitarity and Collinear Limits*, *Nucl. Phys.* **B425** (1994) 217–260, [[hep-ph/9403226](#)].
- [18] Z. Bern, L. J. Dixon, D. C. Dunbar, and D. A. Kosower, *Fusing gauge theory tree amplitudes into loop amplitudes*, *Nucl.Phys.* **B435** (1995) 59–101, [[hep-ph/9409265](#)].
- [19] R. Britto, F. Cachazo, and B. Feng, *Generalized unitarity and one-loop amplitudes in N=4 super-Yang-Mills*, *Nucl.Phys.* **B725** (2005) 275–305, [[hep-th/0412103](#)].
- [20] W. T. Giele, Z. Kunszt, and K. Melnikov, *Full one-loop amplitudes from tree amplitudes*, *JHEP* **0804** (2008) 049, [[arXiv:0801.2237](#)].
- [21] Z. Bern, L. Dixon, F. Febres Cordero, S. Hche, H. Ita, et al., *Next-to-Leading Order W + 5-Jet Production at the LHC*, *Phys.Rev.* **D88** (2013), no. 1 014025, [[arXiv:1304.1253](#)].
- [22] S. Badger, B. Biedermann, P. Uwer, and V. Yundin, *Next-to-leading order QCD corrections to five jet production at the LHC*, *Phys.Rev.* **D89** (2014), no. 3 034019, [[arXiv:1309.6585](#)].
- [23] C. Anastasiou, E. W. N. Glover, C. Oleari, and M. E. Tejeda-Yeomans, *Two loop QCD corrections to massless identical quark scattering*, *Nucl. Phys.* **B601** (2001) 341–360, [[hep-ph/0011094](#)].
- [24] C. Anastasiou, E. W. N. Glover, C. Oleari, and M. E. Tejeda-Yeomans, *Two-loop QCD corrections to the scattering of massless distinct quarks*, *Nucl. Phys.* **B601** (2001) 318–340, [[hep-ph/0010212](#)].
- [25] C. Anastasiou, E. W. N. Glover, C. Oleari, and M. E. Tejeda-Yeomans, *Two loop*

- QCD corrections to massless quark gluon scattering*, *Nucl. Phys.* **B605** (2001) 486–516, [[hep-ph/0101304](#)].
- [26] L. W. Garland, T. Gehrmann, E. W. N. Glover, A. Koukoutsakis, and E. Remiddi, *Two loop QCD helicity amplitudes for $e^+ e^- \rightarrow j$ three jets*, *Nucl. Phys.* **B642** (2002) 227–262, [[hep-ph/0206067](#)].
- [27] L. W. Garland, T. Gehrmann, E. W. N. Glover, A. Koukoutsakis, and E. Remiddi, *The Two loop QCD matrix element for $e^+ e^- \rightarrow j$ 3 jets*, *Nucl. Phys.* **B627** (2002) 107–188, [[hep-ph/0112081](#)].
- [28] T. Gehrmann, M. Jaquier, E. Glover, and A. Koukoutsakis, *Two-Loop QCD Corrections to the Helicity Amplitudes for $H \rightarrow 3$ partons*, *JHEP* **1202** (2012) 056, [[arXiv:1112.3554](#)].
- [29] T. Gehrmann, A. von Manteuffel, and L. Tancredi, *The two-loop helicity amplitudes for $q\bar{q}' \rightarrow V_1 V_2 \rightarrow 4$ leptons*, [arXiv:1503.04812](#).
- [30] A. von Manteuffel and L. Tancredi, *The two-loop helicity amplitudes for $gg \rightarrow V_1 V_2 \rightarrow 4$ leptons*, *JHEP* **1506** (2015) 197, [[arXiv:1503.08835](#)].
- [31] F. Caola, J. M. Henn, K. Melnikov, A. V. Smirnov, and V. A. Smirnov, *Two-loop helicity amplitudes for the production of two off-shell electroweak bosons in gluon fusion*, *JHEP* **1506** (2015) 129, [[arXiv:1503.08759](#)].
- [32] F. Caola, J. M. Henn, K. Melnikov, A. V. Smirnov, and V. A. Smirnov, *Two-loop helicity amplitudes for the production of two off-shell electroweak bosons in quark-antiquark collisions*, *JHEP* **1411** (2014) 041, [[arXiv:1408.6409](#)].
- [33] K. G. Chetyrkin and F. V. Tkachov, *Integration by Parts: The Algorithm to Calculate beta Functions in 4 Loops*, *Nucl. Phys.* **B192** (1981) 159–204.
- [34] F. V. Tkachov, *A Theorem on Analytical Calculability of Four Loop Renormalization Group Functions*, *Phys. Lett.* **B100** (1981) 65–68.
- [35] Z. Bern, L. J. Dixon, and D. Kosower, *A Two loop four gluon helicity amplitude in QCD*, *JHEP* **0001** (2000) 027, [[hep-ph/0001001](#)].
- [36] Z. Bern, A. De Freitas, and L. J. Dixon, *Two loop amplitudes for gluon fusion into two photons*, *JHEP* **09** (2001) 037, [[hep-ph/0109078](#)].
- [37] Z. Bern, A. De Freitas, L. J. Dixon, and H. Wong, *Supersymmetric regularization, two loop QCD amplitudes and coupling shifts*, *Phys.Rev.* **D66** (2002) 085002, [[hep-ph/0202271](#)].
- [38] Z. Bern, A. De Freitas, and L. J. Dixon, *Two loop helicity amplitudes for gluon-gluon scattering in QCD and supersymmetric Yang-Mills theory*, *JHEP* **03** (2002) 018, [[hep-ph/0201161](#)].
- [39] Z. Bern, A. De Freitas, and L. J. Dixon, *Two loop helicity amplitudes for quark gluon scattering in QCD and gluino gluon scattering in supersymmetric Yang-Mills theory*, *JHEP* **0306** (2003) 028, [[hep-ph/0304168](#)].

- [40] A. De Freitas and Z. Bern, *Two-loop helicity amplitudes for quark-quark scattering in QCD and gluino-gluino scattering in supersymmetric Yang-Mills theory*, *JHEP* **0409** (2004) 039, [[hep-ph/0409007](#)].
- [41] D. A. Kosower and K. J. Larsen, *Maximal Unitarity at Two Loops*, *Phys.Rev.* **D85** (2012) 045017, [[arXiv:1108.1180](#)].
- [42] D. Forde, *Direct extraction of one-loop integral coefficients*, *Phys.Rev.* **D75** (2007) 125019, [[arXiv:0704.1835](#)].
- [43] S. Caron-Huot and K. J. Larsen, *Uniqueness of two-loop master contours*, *JHEP* **10** (2012) 026, [[arXiv:1205.0801](#)].
- [44] H. Johansson, D. A. Kosower, and K. J. Larsen, *Two-Loop Maximal Unitarity with External Masses*, *Phys. Rev.* **D87** (2013), no. 2 025030, [[arXiv:1208.1754](#)].
- [45] H. Johansson, D. A. Kosower, and K. J. Larsen, *Maximal Unitarity for the Four-Mass Double Box*, *Phys.Rev.* **D89** (2014) 125010, [[arXiv:1308.4632](#)].
- [46] M. Søgaard, *Global Residues and Two-Loop Hepta-Cuts*, *JHEP* **1309** (2013) 116, [[arXiv:1306.1496](#)].
- [47] M. Søgaard and Y. Zhang, *Multivariate Residues and Maximal Unitarity*, *JHEP* **1312** (2013) 008, [[arXiv:1310.6006](#)].
- [48] M. Søgaard and Y. Zhang, *Unitarity Cuts of Integrals with Doubled Propagators*, *JHEP* **1407** (2014) 112, [[arXiv:1403.2463](#)].
- [49] M. Søgaard and Y. Zhang, *Massive Nonplanar Two-Loop Maximal Unitarity*, *JHEP* **1412** (2014) 006, [[arXiv:1406.5044](#)].
- [50] M. Søgaard and Y. Zhang, *Elliptic Functions and Maximal Unitarity*, *Phys.Rev.* **D91** (2015), no. 8 081701, [[arXiv:1412.5577](#)].
- [51] P. Mastrolia and G. Ossola, *On the Integrand-Reduction Method for Two-Loop Scattering Amplitudes*, *JHEP* **1111** (2011) 014, [[arXiv:1107.6041](#)].
- [52] S. Badger, H. Frellesvig, and Y. Zhang, *Hepta-Cuts of Two-Loop Scattering Amplitudes*, *JHEP* **1204** (2012) 055, [[arXiv:1202.2019](#)].
- [53] Y. Zhang, *Integrand-Level Reduction of Loop Amplitudes by Computational Algebraic Geometry Methods*, *JHEP* **1209** (2012) 042, [[arXiv:1205.5707](#)].
- [54] P. Mastrolia, E. Mirabella, G. Ossola, and T. Peraro, *Scattering Amplitudes from Multivariate Polynomial Division*, *Phys.Lett.* **B718** (2012) 173–177, [[arXiv:1205.7087](#)].
- [55] S. Badger, H. Frellesvig, and Y. Zhang, *An Integrand Reconstruction Method for Three-Loop Amplitudes*, *JHEP* **1208** (2012) 065, [[arXiv:1207.2976](#)].
- [56] P. Mastrolia, E. Mirabella, G. Ossola, and T. Peraro, *Integrand-Reduction for Two-Loop Scattering Amplitudes through Multivariate Polynomial Division*, *Phys.Rev.* **D87** (2013), no. 8 085026, [[arXiv:1209.4319](#)].

- [57] P. Mastrolia, E. Mirabella, G. Ossola, and T. Peraro, *Multiloop Integrand Reduction for Dimensionally Regulated Amplitudes*, *Phys.Lett.* **B727** (2013) 532–535, [[arXiv:1307.5832](#)].
- [58] S. Badger, H. Frellesvig, and Y. Zhang, *A Two-Loop Five-Gluon Helicity Amplitude in QCD*, *JHEP* **1312** (2013) 045, [[arXiv:1310.1051](#)].
- [59] Z. Bern, J. Carrasco, and H. Johansson, *New Relations for Gauge-Theory Amplitudes*, *Phys.Rev.* **D78** (2008) 085011, [[arXiv:0805.3993](#)].
- [60] Z. Bern, J. J. M. Carrasco, and H. Johansson, *Perturbative Quantum Gravity as a Double Copy of Gauge Theory*, *Phys.Rev.Lett.* **105** (2010) 061602, [[arXiv:1004.0476](#)].
- [61] Z. Bern, J. Carrasco, L. J. Dixon, H. Johansson, and R. Roiban, *The Complete Four-Loop Four-Point Amplitude in $N=4$ Super-Yang-Mills Theory*, *Phys.Rev.* **D82** (2010) 125040, [[arXiv:1008.3327](#)].
- [62] Z. Bern, M. Czakon, D. A. Kosower, R. Roiban, and V. A. Smirnov, *Two-loop iteration of five-point $N=4$ super-Yang-Mills amplitudes*, *Phys. Rev. Lett.* **97** (2006) 181601, [[hep-th/0604074](#)].
- [63] J. J. Carrasco and H. Johansson, *Five-Point Amplitudes in $N=4$ Super-Yang-Mills Theory and $N=8$ Supergravity*, *Phys.Rev.* **D85** (2012) 025006, [[arXiv:1106.4711](#)].
- [64] N. Arkani-Hamed, J. L. Bourjaily, F. Cachazo, S. Caron-Huot, and J. Trnka, *The All-Loop Integrand For Scattering Amplitudes in Planar $N=4$ SYM*, *JHEP* **1101** (2011) 041, [[arXiv:1008.2958](#)].
- [65] J. L. Bourjaily and J. Trnka, *Local Integrand Representations of All Two-Loop Amplitudes in Planar SYM*, [arXiv:1505.05886](#).
- [66] N. Arkani-Hamed, J. L. Bourjaily, F. Cachazo, A. Postnikov, and J. Trnka, *On-Shell Structures of MHV Amplitudes Beyond the Planar Limit*, *JHEP* **06** (2015) 179, [[arXiv:1412.8475](#)].
- [67] S. Franco, D. Galloni, B. Penante, and C. Wen, *Non-Planar On-Shell Diagrams*, *JHEP* **06** (2015) 199, [[arXiv:1502.02034](#)].
- [68] Z. Bern, L. J. Dixon, D. C. Dunbar, and D. A. Kosower, *One loop selfdual and $N=4$ superYang-Mills*, *Phys.Lett.* **B394** (1997) 105–115, [[hep-th/9611127](#)].
- [69] R. Kleiss and H. Kuijf, *Multi - Gluon Cross-sections and Five Jet Production at Hadron Colliders*, *Nucl.Phys.* **B312** (1989) 616.
- [70] V. Del Duca, A. Frizzo, and F. Maltoni, *Factorization of tree QCD amplitudes in the high-energy limit and in the collinear limit*, *Nucl.Phys.* **B568** (2000) 211–262, [[hep-ph/9909464](#)].
- [71] V. Del Duca, L. J. Dixon, and F. Maltoni, *New color decompositions for gauge amplitudes at tree and loop level*, *Nucl.Phys.* **B571** (2000) 51–70, [[hep-ph/9910563](#)].

- [72] S. Badger, H. Frellesvig, and Y. Zhang, *Multi-loop Integrand Reduction with Computational Algebraic Geometry*, [arXiv:1310.4445](#).
- [73] W. van Neerven and J. Vermaseren, *Large Loop Integrals*, *Phys.Lett.* **B137** (1984) 241.
- [74] R. Britto, F. Cachazo, and B. Feng, *New recursion relations for tree amplitudes of gluons*, *Nucl.Phys.* **B715** (2005) 499–522, [[hep-th/0412308](#)].
- [75] R. Britto, F. Cachazo, B. Feng, and E. Witten, *Direct proof of tree-level recursion relation in Yang-Mills theory*, *Phys.Rev.Lett.* **94** (2005) 181602, [[hep-th/0501052](#)].
- [76] S. Catani, S. Dittmaier, and Z. Trocsanyi, *One loop singular behavior of QCD and SUSY QCD amplitudes with massive partons*, *Phys. Lett.* **B500** (2001) 149–160, [[hep-ph/0011222](#)].
- [77] A. V. Smirnov, *FIESTA 3: cluster-parallelizable multiloop numerical calculations in physical regions*, *Comput. Phys. Commun.* **185** (2014) 2090–2100, [[arXiv:1312.3186](#)].
- [78] S. Borowka, G. Heinrich, S. P. Jones, M. Kerner, J. Schlenk, and T. Zirke, *SecDec-3.0: numerical evaluation of multi-scale integrals beyond one loop*, [arXiv:1502.06595](#).
- [79] C. D. White, *An Introduction to Webs*, [arXiv:1507.02167](#).
- [80] R. Lee, *Presenting LiteRed: a tool for the Loop InTEgrals REDuction*, [arXiv:1212.2685](#).
- [81] A. V. Smirnov, *FIRE5: a C++ implementation of Feynman Integral REDuction*, *Comput. Phys. Commun.* **189** (2014) 182–191, [[arXiv:1408.2372](#)].
- [82] T. Gehrmann and E. Remiddi, *Two loop master integrals for $\gamma^* \rightarrow 3$ jets: The Planar topologies*, *Nucl. Phys.* **B601** (2001) 248–286, [[hep-ph/0008287](#)].
- [83] T. Gehrmann and E. Remiddi, *Two loop master integrals for $\gamma^* \rightarrow 3$ jets: The Nonplanar topologies*, *Nucl. Phys.* **B601** (2001) 287–317, [[hep-ph/0101124](#)].